Bull. Chem. Soc. Ethiop. **2023**, 37(2), 463-476.
DOI: https://dx.doi.org/10.4314/bcse.v37i2.15

ISSN 1011-3924
Printed in Ethiopia
Online ISSN 1726-801X

EFFECT OF SYNTHESIZED CARBON QUANTUM DOTS ON THE PHOTOCATALYTIC PROPERTIES OF ZnO

Irié Bi Irié Williams[1,2], Essy Kouadio Fodjo[2*], Pomi Bi Boussou Narcisse[2], Aka Alla Martin[2], Koffi Koffi Kra Sylvestre[2], Trokourey Albert[2] and Zhen Gu[1*]

[1]Key Laboratory of Advanced Control and Optimization for Chemical Processes Ministry of Education, East China University of Science and Technology, Shanghai 200237, China
[2]Laboratory of Constitution and Reaction of Matter, UFR SSMT, Université Felix Houphouet Boigny, 22 BP 582 Abidjan 22, Cote d'Ivoire

(Received January 10, 2022; Revised September 21, 2022; Accepted September 23, 2022)

ABSTRACT. In this work, synthesized carbon quantum dots (CQDs) and zinc oxide nanoparticles (ZnO NPs) are used to form ZnO/CQDs nanocomposite. The characterization of this nanocomposite using X-ray diffraction (XRD) indicates that ZnO NPs and ZnO/CQDs nanocomposite have the same profile, suggesting that the presence of CQDs does not impinge the crystal structure of ZnO in ZnO/CQDs nanocomposite. Besides, an analysis performed with scanning electron microscopy (SEM) displays plate-like nanostructure with an average thickness of about 22 nm and 25 nm for ZnO NPs and ZnO/CQDs, respectively. Furthermore, the reflectance study in the visible range shows a reduction of sunlight reflection intensity of ZnO/CQDs compared with the reflection intensity of ZnO NPs. In addition, the photocatalytic studies indicate that the rate of photocatalytic degradation of methylene blue (MB) of ZnO/CQDs nanocomposites is higher than that of ZnO NPs. Indeed, in optimized conditions, the photocatalytic activity can reach 100% within 45 min of sunlight exposure for the degradation of 7.5 mg/L MB using ZnO/CQDs while it takes 90 min using ZnO NPs under the same conditions. These fascinating results is attributed to the reduction of the reflective properties of ZnO/CQDs.

KEY WORDS: Fluorescent carbon quantum dots (CQDs), Photocatalytic degradation of methylene blue, Sunlight reflectance property, Synthesis of ZnO nanoparticles

INTRODUCTION

Industrialization and continued population growth are supported by increasing use of chemicals. These chemicals are mostly source of pollution, particularly the water pollution [1, 2]. This water pollution has reached its peak with the production of colored water in the areas where certain anthropogenic activities such as agriculture with the use of fertilizers, or the industrial activities making food, tannery, and pulp products are carried out. This pollution, although endangering human life, predominantly threatens environmental and aquatic life [3, 4]. As a result, water quality and availability continue to deteriorate as the colored water prevents the process of aquatic photosynthesis. Owing to the complexity of the different types of pollutants, the implementation of simple, fast, effective, and low-cost treatment techniques of these pollutants in wastewater remains a major challenge. To contain this plague, several techniques such as adsorption [5], biosorption [6], and coagulation [7] are used. However, these wastewater treatment methods transfer the pollution from an aqueous phase to a new phase, leading mostly to a formation of concentrated sludge, thus creating secondary pollution. The photocatalysis process is one of the most promising methods for sustainable wastewater treatment, especially for the degradation of organic dyes. In this process, the dye is directly converted into non-toxic by-products such as H_2O without secondary water pollution. In addition, photocatalysis is beneficial as a small amount of photocatalyst is needed for the abundant and available sunlight which is the light source [1]. As one of the most widely used semiconductors, zinc oxide (ZnO) is considered as an effective photocatalyst for the degradation of organic pollutants [8]. Indeed, ZnO nanoparticles (ZnO NPs)

*Corresponding author. E-mail: kouadio.essy@univ-fhb.edu.ci (E.K.), guzhen@ecust.edu.cn (Z.G.)

are especially used in the field of photocatalysis because of its stable physical and chemical properties, its non-toxicity, and relatively low cost [9-11]. Because of these characteristics, ZnO NPs are considered as a substitutable substrate for TiO_2 in the field of photocatalysis [12]. However, ZnO has a broad band gap (3.37 eV) which significantly confines its use as a photocatalyst in UV region [13]. Despite this limitation, the band gap can be adjusted at nanoscale by doping ZnO with other chemicals to improve its properties [14]. In addition, carbonaceous materials such as carbon nitride, carbon nanotubes, and graphene have also been the subject of investigation to adequately dope ZnO [15]. For this purpose, carbon quantum dots (CQDs) have experienced a remarkable interest in the carbon family especially due to their optical and electronic properties, as well as their excellent biocompatibility, high aqueous solubility, and low toxicity [16, 17]. These impeccable properties make them ideal candidates for applications in the fields such as biomedical, optoelectronics, and photocatalysis [18]. In this regard, CQDs prepared by a green method in our previous work were used to fabricate ZnO/CQDs nanocomposite [19]. Indeed, doping of ZnO with CQDs promotes photogenerated electrons from the valence band to the conduction band. In this current work, CQDs were obtained from chemical fragmentation using charcoal as a carbon source. These CQDs were used to design nanostructured ZnO/CQDs and applied for the elimination of methylene blue in aqueous environment. The study of the photocatalytic properties showed that ZnO/CQDs have higher degradation rate compared with those of ZnO NPs. This excellent performance could be due to the reduction of reflection properties of ZnO NPs by CQDs in ZnO/CQDs nanocomposites in the visible range. This enhancement of the photocatalytic properties of ZnO NPs using CQDs may offer an innovative approach to produce excellent photocatalysts.

EXPERIMENTAL

Reagents

In this study, the chemicals used were of analytical grade and were used without any further purification. Zinc nitrate hexahydrate ($(Zn(NO_3)_2.6H_2O)$, 98%,) and ammonium hydroxide (NH_4OH, 28-30%) were supplied by Honeywell Fluka (Buchs, Switzerland). Methylene blue ($C_{16}H_{18}ClN_3S$, 98%) was purchased from Merck (Darmstadt, Germany). Ethanol (C_2H_5OH, 98%), hydrochloric acid (HCl, 37%), acetone (C_3H_6O, 98%), and potassium hydroxide (KOH, 85%) were supplied by Panreac quimica (Barcelona, Spain). The deionized (DI) water used in this study was produced by Sichuan Zhuoyue Water Treatment Equipment Co., Ltd. (Chengdu, China). The water purification system can allow obtaining DI water with resistivity of 18.25 MΩ·cm. The charcoal used to prepare the CQDs was obtained from the local market (Abidjan, Cote d'Ivoire).

Synthesis of CQDs, ZnO NPs, and ZnO/CQDs nanocomposites

The CQDs were prepared following the procedure described in the literature [19, 20], using chemical fragmentation method at a relatively low temperature (50 °C). In a typical synthesis procedure, as described in our previous work [19], 50 mL of 2.5 M NH_4OH solution was prepared from commercial NH_4OH by dilution with DI water. Afterwards, 500 mg of powdered charcoal was added to this solution previously adjusted at 50 °C in a water bath under a magnetic stirring at 500 rpm for 10 min and under fume hood, followed by gentle stirring at the same temperature (50 °C) for 12 h. The resulting solution was then cooled to room temperature and centrifuged at 4000 rpm for 5 min using a high-speed bench-top centrifuge (MRC Ltd., Holon, Israel) to remove all particles beyond nanosize. To the recovered supernatant, DI water was added to reach 25 mL. The newly obtained solution was heated again at 50 °C in the water bath under stirring at 500 rpm for 10 min. To this solution, 17 mL of 2.5 M NH_4OH solution was added and filled with DI water to reach a final volume of 50 mL. The obtained solution was kept at 50 °C with gentle stirring for

12 h, followed by its cooling to room temperature, and then centrifuged at 4000 rpm for 5 min to finally obtain the suspension of CQDs.

ZnO NPs were synthesized by precipitation method using zinc nitrate hexahydrate ($Zn(NO_3)_2.6H_2O$) and KOH as precursors [21]. Firstly, 6.093 g of zinc nitrate hexahydrate (0.2 g/L) was dissolved in 100 mL of DI water and kept under constant stirring for 30 min for its complete dissolution. Then, 1.632 g of KOH (0.4 g/L) was dissolved in another 100 mL DI water. Afterwards, this KOH solution was added dropwise to the zinc nitrate solution at room temperature (28 °C) under continuous and vigorous stirring at 500 rpm for 1 h to obtain a white suspended precipitate. The resulting product was centrifuged and washed successively with DI water and ethanol, and then calcined in air at 500 °C for 3 h with a temperature rise of 5 °C/min.

The nanocomposite consisting of CQDs and ZnO NPs (ZnO/CQDs) was synthesized according to the previously described procedure [22]. Briefly, 250 mg of previously synthesized ZnO NPs was dispersed in 125 mL of ethanol and vortexed for 10 min. To this solution, 50 µL of previous colloidal solution of CQDs was added. This mixture was stirred at 500 rpm for 30 min at room temperature. The obtained solution was collected by centrifugation, washed three times with ethanol, and dried at 100 °C for 3 h to finally obtain the ZnO/CQDs nanocomposites.

Characterization of the synthesized nanostructures

X-Ray diffraction (XRD) analysis of the different prepared samples was performed using a Siemens D5005 diffractometer (Simens AG, Munich, Germany) with a copper anticathode ($\lambda_{K\alpha 1}$ = 1.5406 Å). The angle of incidence 2Θ was set to vary from 5° to 90°, with a step size of 0.02. The absorbance and reflectance of these samples were measured with a Flame-S-XR1 UV-Vis spectrometer (Ocean Optics, Largo, USA). Fluorescence test of the synthesized CQDs was done using Qiwei WFH-204B 254/365 nm portable UV lamp (Hangzhou, China). Morphological characterization of ZnO NPs and ZnO/CQDs was performed by scanning electron microscopy (SEM) using JSM-6010LA (JEOL Ltd., Tokyo, Japan).

Photocatalytic analysis

In this study, all photocatalytic experiments were performed between 11:00 AM and 3:00 PM where the sunlight is very intense in order to take maximum advantage of the solar irradiation. To evaluate the photocatalytic properties of ZnO and ZnO/CQDs nanostructures, 150 mg of ZnO NPs (or ZnO/CQDs) was introduced into a beaker containing 100 mL of 7.5 mg/L MB chosen as model of pollutant. This mixture was kept in the dark under magnetic stirring at 500 rpm for 30 min to reach adsorption-desorption equilibrium [23]. Once equilibrium was reached, the mixture was irradiated with sunlight at different times. With the mixture under the sun irradiation, 2 mL of the samples were taken every 30 and 15 min for prepared aqueous MB and wastewater contaminated with MB, respectively, which were finally centrifuged. The remaining MB concentration in the centrifuged solutions was analyzed by measuring the intensity of the absorbance peak at 664 nm (characteristic peak of MB) using Flame-S-XR1 UV-Vis spectrometer (Ocean Optics, Largo, USA). Then, the calculation of the percentage of dye degradation in the presence of ZnO NPs or ZnO/CQDs was evaluated using Equation (1):

$$\%D = \frac{C_0 - C_t}{C_0} \times 100 \quad (1)$$

where C_0 represents the initial concentration of the MB dye and C_t represents its concentration after solar irradiation at a time t.

This procedure was used for the study of the influence of the initial concentration of MB, the catalyst mass, and the pH of the media on the degradation of MB by varying the initial

concentration of MB from 5 mg/L to 15 mg/L, the mass of ZnO NPs from 100 mg to 350 mg and the pH of the media from 2 to 13, respectively.

Kinetic study of MB degradation

To know the kinetic order of the MB degradation reaction, the kinetic study of the photocatalytic reaction of MB was carried out by varying the initial concentration of MB from 5 to 15 mg/L (5, 7.5, 10, 12.5 and 15 mg/L). In detail, a mass of 150 mg of ZnO NPs or ZnO/CQDs was added to 100 mL of MB solution at the above different concentrations. The kinetic order of MB degradation is evaluated using Equations (2) and (3) [24] :
Pseudo-first order kinetic equation:

$$ln\left({}^{C_0}/_{C_t}\right) = k_1 t \quad (2)$$

Pseudo-second order kinetic equation can be formulated using Equation (3):

$${}^{1}/_{C_t} - {}^{1}/_{C_0} = k_2 t \quad (3)$$

where C_0 and C_t are the initial and different time t concentration of MB, respectively. k_1 and k_2 are the rate constants for the pseudo-first-order and pseudo-second-order models, respectively.
The study of MB adsorption isotherms on ZnO NPs and ZnO/CQDs was performed for the following models:
• Langmuir-Hinshelwood model: Langmuir-Hinshelwood model is widely used to describe the experimental results in heterogeneous photocatalysis. This model is expressed by Equation (2).
• Temkin model: Temkin isotherm accounts for the fact that the heat of adsorption of all molecules in the capping layer decreases linearly with capping due to the decrease in adsorbent-adsorbate interactions. The adsorption is characterized by a uniform distribution of surface binding energies. This isotherm is expressed with Equation (4) [25]:

$$q_e = (RT/b_t) \cdot ln(K_t \cdot C_e) \quad (4)$$

Or in the form of Equation (5):

$$q_e = B_1 \cdot lnK_t + B_1 \cdot lnC_e \quad (5)$$

with B_1, the Temkin's constant for the heat of adsorption and K_t ($L.g^{-1}$), the adsorption equilibrium constant corresponding to the maximum binding energy.
• Langmuir model: Langmuir model is valid for a monolayer adsorption with a finite number of identical sites. This model is associated to Equation (6):

$$1/q_e = 1/q_m + (1/q_m K_L)\ 1/C_e \quad (6)$$

with q_m ($mg.g^{-1}$) the maximum rate of adsorbate per unit mass of the adsorbent; K_L ($L.mg^{-1}$) the Langmuir adsorption equilibrium constant; C_e the concentration of the solution at equilibrium.
• Freundlich model: Freundlich model is an empirical model based on adsorption on heterogeneous surfaces. This isotherm is expressed by Equation (7):

$$lnq_e = lnK_F + (1/n)\ lnC_e \quad (7)$$

with K_F ($mg.g^{-1}(mgL^{-1})^{-1/n}$) the Freundlich adsorption constant and n a constant depending on the nature of the adsorbate and the temperature.

Application

In order to evaluate the applicability of the synthesized ZnO NPs and ZnO/CQDs in a real sample, wastewater from the University Hospital of Cocody (UHC) was examined with and without its

contamination by MB. The wastewater samples were collected from UHC and then transferred to a one-liter polyethylene canister, stored at 4 °C and protected from light in a cooler containing ice to avoid possible photochemical reactions. The samples were then transported to the laboratory and stored in a refrigerator at 4 °C.

RESULTS AND DISCUSSION

Characterization of the synthesized nanostructures

In order to know the characteristics of the prepared nanostructures, the XRD analysis of ZnO NPs and ZnO/CQDs has been done (Figure 1a). The results of the obtained diffraction patterns show diffraction peaks associated to hexagonal wurtzite structure with mesh parameters of a = b = 3.2498 Å, and c = 5.2066 Å, which are in good agreement with the data sheet (JCPDS No. 36-1451). The inset spectrum displays a typical broad diffraction peak of CQDs from 10° to 25° assigned to disordered graphitic structure [26]. Additionally, the results clearly show that there is no presence of extra peak on the diffractogram of ZnO/CQDs compared to those of ZnO NPs, suggesting that the two prepared catalysts have similar crystal structures. It is obvious that the presence of CQDs does not affect ZnO NPs structure as already demonstrated in the literature [27]. However, the slight decrease in the peak intensity of the different ZnO/CQDs diffraction peaks denote that ZnO NPs is highly crystalline than ZnO/CQDs. All these results suggest that the CQDs are deposited on ZnO NPs surface in the ZnO/CQDs nanocomposite system [28]. Using Debye-Scherrer equation (Equation 8), the particle sizes are found to be around 22 nm and 25 nm for ZnO NPs and ZnO/CQDs, respectively:

$$D_{hkl} = \frac{0.9\lambda}{\beta_{hkl} cos\theta_{hkl}} \quad (8)$$

where D_{hkl} is the grain size (in nm); λ is the wavelength of the X-ray beam; θ_{hkl} is the diffraction angle; and β_{hkl} is the half-value width expressed in radians for hkl.

To further examine the effect of CQDs in ZnO/CQDs nanocomposites, the reflectance of ZnO NPs and ZnO/CQDs was studied in the UV-Vis range. The obtained results (Figure 1b) show that the reflectance of ZnO NPs is significantly higher than that of ZnO/CQDs nanocomposites in the visible range. This decrease in the reflectance properties of ZnO/CQDs denotes that the doping of ZnO NPs with CQDs leads to an important reduction in the reflection of light rays by ZnO NPs in the visible range. Therefore, the photocatalytic performance of ZnO/CQDs can be better than that of ZnO NPs alone under visible light irradiation as explained in the literature [28].

Furthermore, to investigate the morphology of synthesized nanomaterials, the characterization of the prepared nanomaterials was done using SEM. Figures 1c and 1d show the SEM images of ZnO NPs and ZnO/CQDs, respectively. The results indicate that these substrates are nanometric in size with polydisperse shapes consisting of nanosheets for ZnO NPs and ZnO/CQDs. These different forms can play an important role in their catalytic application as suggested in the literature [29].

MB degradation using the synthesized nanostructures as catalyst under solar irradiation

In order to evaluate the photocatalytic properties of the ZnO NPs and ZnO/CQDs, the degradation of MB in aqueous medium was examined (Figure 1e). As presented in this Figure, the MB absorption peak intensity rapidly decreases during the first 30 min of sun irradiation in the presence of ZnO NPs followed by its disappearance after 180 min of irradiation **(**Figures 1f and 1g), while in the presence of ZnO/CQDs, the same peak undergoes a rapid decrease in the first 30 min and completely disappears in 120 min. This disappearance of the peak indicates the degradation of MB by ZnO NPs and ZnO/CQDs, showing the excellent photocatalytic properties of ZnO NPs and ZnO/CQDs for the MB degradation in aquatic environment [27]. However,

ZnO/CQDs are the best photocatalysts with shorter degradation time. This result is in good agreement with the obtained reflectance results.

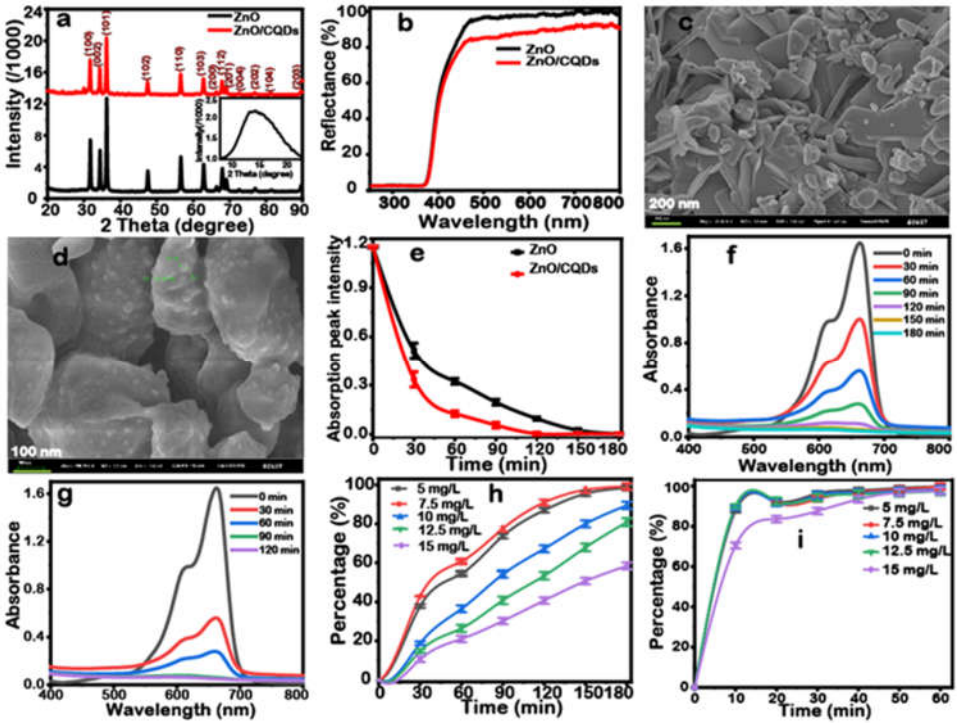

Figure 1. a) XRD spectra (inset: XRD spectrum of CQDs), and b) reflectance spectra of ZnO NPs and ZnO/CQDs. SEM images of c) ZnO NPs and d) ZnO/CQDs. e) Degradation of 7.5 mg/L MB under solar irradiation using ZnO NPs and ZnO/CQDs. UV-Vis spectra at different times of MB using f) ZnO NPs and g) ZnO/CQDs. Percentage of removed MB at different times with h) ZnO NPs and i) ZnO/CQDs.

Influence of initial MB concentration on its degradation rate

To investigate the influence of the initial MB concentration on its removal rate, different initial MB concentrations were examined (Figures 1h and 1i). The results show that the percentage of MB removal decreases with increasing initial MB concentration. This effect is due to the fact that once the entire surface of the photocatalyst is covered by the molecules of MB, the extra MB molecules prevent the sunlight from reaching the photocatalyst surface, reducing the production of $^{\bullet}OH$ radicals [30].

Influence of ZnO NPs mass on MB degradation rate

In an effort to determine the optimal mass of ZnO NPs upon photocatalytic removal of MB, experiments were performed in the presence of different masses of ZnO NPs under sunlight (Figure 2a). These results show that the MB degradation time is shorter for 150 mg than that of a

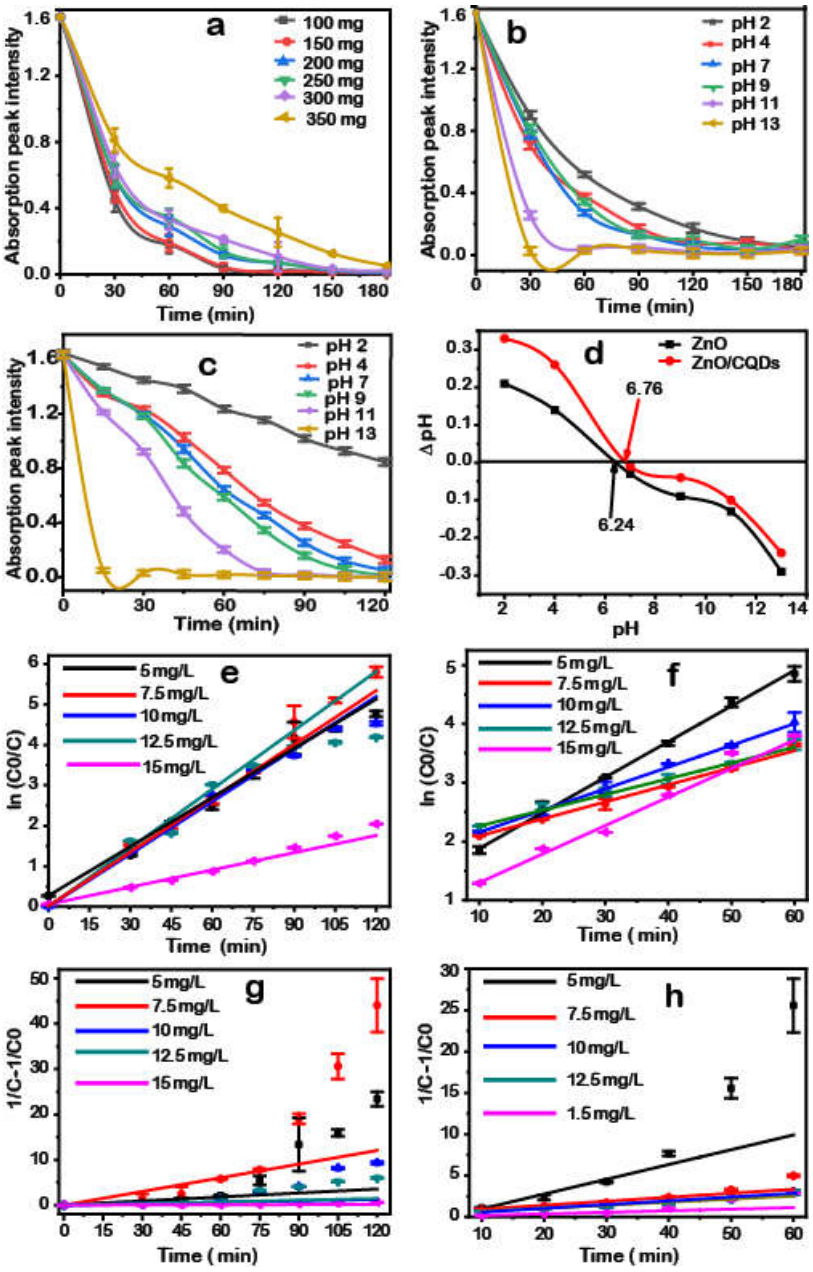

Figure 2. a) 7.5 mg/L MB degradation at different times for different masses of ZnO NPs. Effect of pH on the 7.5 mg/L MB degradation with b) ZnO NPs and c) ZnO/CQDs. d) pH variation as a function of the initial pH of ZnO and ZnO/CQDs. Degradation kinetics for pseudo-first order and pseudo-second order for (e, g) ZnO NPs and (f, h) ZnO/CQDs, respectively.

lower or higher mass, indicating that 150 mg is the optimal mass. However, for a mass greater than 150 mg, a complete removal of MB is possible only after a long solar exposure. This result can be justified by the turbidity of the solution, which reduces the efficiency of the catalytic reaction [19]. At 150 mg, a large amount of photogenerated active species ($^{\bullet}OH$ and h^+), which are responsible of the catalytic activities of the synthesized nanostructures, are produced in the medium.

Influence of pH on the MB degradation rate

In order to evaluate the influence of pH on the degradation efficiency of MB in the presence of ZnO NPs and ZnO/CQDs, a series of experiments were performed at different pH (Figures 2b and 2c). The results show that the percentage of removed MB increases with the increase in pH in both cases, and 100% of removal is obtained at higher pH after 90 min and 45 min for ZnO NPs and ZnO/CQDs, respectively. Indeed, this result is made possible by the attractive electrostatic interactions between the electrophilic sites of the MB and the nucleophilic sites of the photocatalysts [31]. To further understand this effect of pH, the zero charge point (PZC) of ZnO NPs or ZnO/CQDs was evaluated. To achieve these objectives, 20 mg of ZnO NPs or ZnO/CQDs were dissolved in 20 mL of an aqueous solution of 0.1 M KNO_3 and adjusted to different pH ranging from 2 to 13. The suspension was stirred for 24 h at room temperature (28 °C). The final pH of the solution was measured. The difference between the final pH and the initial pH (ΔpH) was plotted against the initial pH of the solution (Figure 2d). The intersection of this curve with the x-axis corresponds to the PZC (pHpzc) [31]. The results obtained indicate that the pHpzc of ZnO and ZnO/CQDs are around 6.2 and 6.8, respectively. These results confirm the good catalytic activities of ZnO and ZnO/CQDs in alkaline media. Above pHpzc, the surface of the photocatalyst is negatively charged and thus a strong attraction takes place between the surface of the photocatalyst and the MB molecules (cationic). Due to this attractive interaction, the dye molecules are adsorbed on the photocatalyst surface, which results in a higher degradation efficiency as displayed by the reaction mechanism described by Equations (9-16) [27]. It should be noted that this adsorption of MB on the photocatalyst surface in alkaline medium is mainly due to the presence of OH^- ions on the surface of the photocatalysts [30, 32].

$$ZnO + h\vartheta \rightarrow ZnO(e^-(BC) + h^+(BV)) \quad (9)$$

or

$$ZnO/CQDs + h\vartheta \rightarrow ZnO/CQDs\ (e^-(BC) + h^+(BV)) \quad (10)$$

$$e^-(BC) \rightarrow e^-(CQDs) \quad (11)$$

$$e^-(CQDs) + O_2 \rightarrow O_2^{\bullet -} \quad (12)$$

$$h^+(BV) + H_2O \rightarrow H^+ + OH^{\bullet} \quad (13)$$

$$2OH^{\bullet} \rightarrow H_2O_2 \quad (14)$$

$$H_2O_2 + O_2^{\bullet -} \rightarrow OH^{\bullet} + OH^- + O_2 \quad (15)$$

$$MB + (OH^{\bullet}, O_2^{\bullet -}) \rightarrow CO_2 + H_2O \quad (16)$$

During the exposure of the sample to sunlight, the incident beam with energy above the band gap of ZnO causes interfacial electron transfer between the oxygen vacancies and the interstitial zinc atom, leaving electrons in the conduction band (CB) and holes in the valence band (VB) [33]. With the presence of CQDs onto ZnO NPs, the electrons from ZnO CB are transferred to the CQDs, resulting in efficient separation of the light-generated electron and hole pairs, enhancing therefore the photocatalytic performance of the nanocomposite. The generated holes (h^+) react

with the adhered water molecules on the ZnO surface to produce reactive hydroxyl radicals ($HO^{\bullet}$). Similarly, the electrons (e^-) react with oxygen and reduce the oxygen molecules to superoxide radical anions ($O_2^{\bullet -}$) [34]. These two oxygen species are responsible of the photocatalytic activity of ZnO/CQDs.

Kinetics of MB degradation

Study of the effect of the variation of the initial MB concentration on the rate of MB degradation, in the presence of ZnO NPs and ZnO/CQDs was carried out to assess the kinetic of MB degradation. The values of the photodegradation kinetic constants of MB dye are determined using Equations (2) and (3) for pseudo first order (Figures 2e and 2g) and pseudo second order (Figures 2f and 2h) in the presence of ZnO NPs and ZnO/CQDs, respectively. The results of the rate constants k_1, k_2, and the different correlation coefficients R^2 are recorded in Table 1. As displayed, R^2 values are clearly closer to 1 for the pseudo first order than those obtained in the case of the pseudo second order in the presence of both photocatalysts (ZnO NPs and ZnO/CQDs). These results denote that the degradation of MB follows apparent pseudo first order kinetics.

Table 1. Kinetic parameters of MB degradation.

Initial concentration of MB (mg/L)	Pseudo-first order				Pseudo-second order			
	k_1 (min^{-1})		R^2		k_2 (min^{-1})		R^2	
	a*	b*	a*	b*	a*	b*	a*	b*
5	0.0255	0.1053	0.9969	0.9777	0.0099	0.0048	0.8671	0.6716
7.5	0.0139	0.1298	0.9888	0.9995	0.0041	0.0104	0.8669	0.8548
10	0.0168	0.1443	0.9863	0.9659	0.0026	0.0115	0.8808	0.4185
12.5	0.0149	0.1169	0.9700	0.9772	0.0034	0.0110	0.8943	0.8184
15	0.0153	0.0888	0.9583	0.9483	0.0025	0.0050	0.9661	0.7006

a*: ZnO NPs and b*: ZnO/CQDs.

Table 2. Equilibrium parameters of MB adsorption isotherms on ZnO NPs and ZnO/CQDs.

Models	R^2		K_{L-H}		lnk_t		B_1		K_L		lnK_F	
	a*	b*	a*	b*	a*	b*	a*	b*	a*	b*	a*	b*
Langmuir-Hinshewood	0.9897	0.9989	0.0430	0.0268								
Temkin	0.9040	0.9500			-2.488	-14.37	-1.739	-0.307				
Langmuir	0.4872	0.8113							-715.307	-45.400		
Freundlich	0.8420	0.9507									1.364	1.483

a*: ZnO NPs and b*: ZnO/CQDs

Furthermore, for a better description of the MB degradation phenomenon, the study of MB adsorption isotherms in the presence of ZnO NPs and ZnO/CQDs was also examined by performing Langmuir-Hinshelwood and Temkin isotherms (Figures 3a-3d), and those of Langmuir and Freundlich (Figures 3e-3h). The results recorded in Table 2 clearly suggest that the Langmuir-Hinshelwood kinetic model shows better agreement for the MB degradation kinetics as R^2 are closer to 1, indicating that the MB degradation occurs at the photocatalyst surface. These results confirm the results obtained from the studies of the effect of pH. Indeed, during the MB degradation mechanism, the molecules absorbed at the photocatalyst surface undergo a

bimolecular reaction at the nearest nucleophilic sites [35]. On the other hand, the correlation coefficients obtained in the case of Temkin's kinetic model are 0.90 and 0.95 using ZnO NPs and ZnO/CQDs as photocatalysts, respectively. These values of R^2 are also relatively close to 1, indicating that the degradation of MB on ZnO NPs and ZnO/CQDs photocatalysts can also be described by Temkin kinetic model while in general, those obtained from Langmuir and Freundlich are a little bit far from 1 and divaricate. It appears from this study that the removal of MB is described by Langmuir-Hinshelwood and Temkin type adsorption isotherms using ZnO NPs and ZnO/CQDs.

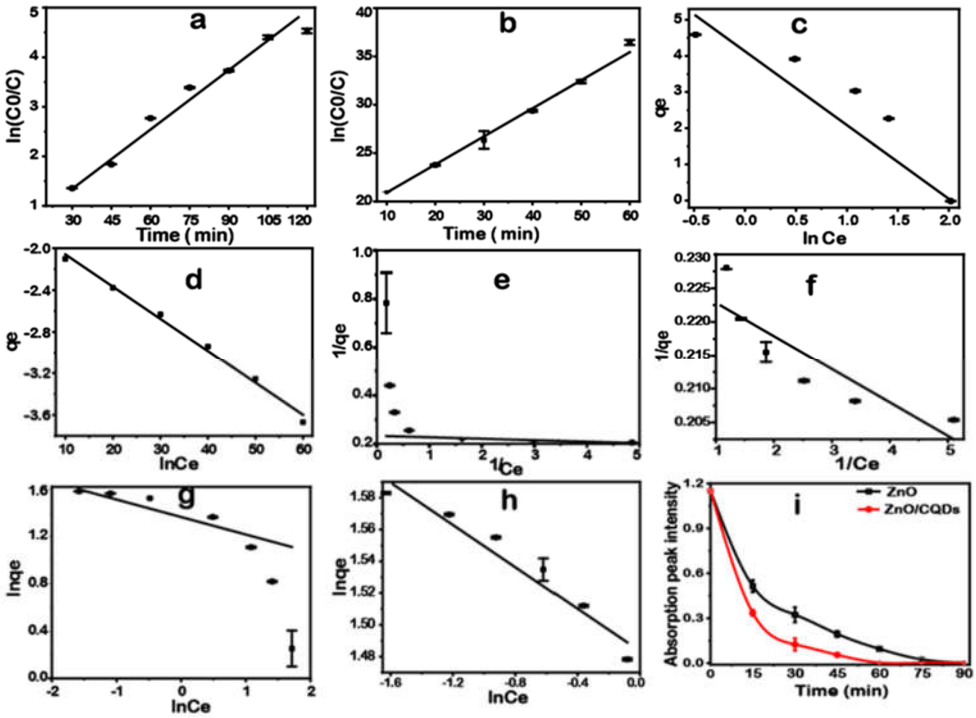

Figure 3. Adsorption models of Langmuir-Hinshelwood for a) ZnO NPs and b) ZnO/CQDs, and Temkin for c) ZnO NPs and d) ZnO/CQDs. Adsorption models with (e and f) Langmuir and, with (g and h) Freundlich over 150 mg for ZnO NPs and ZnO/CQDs, respectively. i) UHC wastewater degradation after the addition of MB, using ZnO NPs and ZnO/CQDs as photocatalyst. A concentration of 7.5 mg/L MB was used for these experiments.

Application

In order to evaluate the photocatalytic efficiency of ZnO NPs and ZnO/CQDs in a real solution, the wastewater of UHC was evaluated before and after its MB contamination. Before any measurements, the wastewater samples were decanted and filtered using a 0.45 µm diameter FILTER LAB filter. This collected water is yellow in color (Figure 4c and 4d) with a temperature of 27.6 °C, pH of 8.4, conductivity of 836 µS/cm, and water salinity of 1.7. Since electric current is carried by ions in solution, this high conductivity denotes that this UHC wastewater contains a

high amount of ions. Furthermore, the measurement of the absorbance of this water sample shows a broad adsorption band between 200 and 400 nm (Figure 4a and 4b), confirming the contamination of UHC water. The monitoring of the discoloration of this wastewater by the synthesized nanostructures without addition of the MB is indicated in Figures 4c and 4d. As displayed, the color of this water sample disappears within an hour suggesting that ZnO NPs and ZnO/CQDs are excellent photocatalysts for the treatment of the wastewater. Moreover, after the UHC water contamination with MB (Figures 5), the characteristic peak of MB around 664 nm (Figure 3i and Figures 5a and 5b) and discoloration of the contaminated water (Figures 5c and 5d) were followed in the presence of 150 mg of ZnO NPs or ZnO/CQDs photocatalysts under solar irradiation at room temperature. After 60 min and 45 min, a total discoloration of these wastewater samples was observed in the presence of ZnO NPs and ZnO/CQDs, respectively. It is evident from these results that a better MB degradation or other pollutant degradation is observed in the case of ZnO/CQDs, confirming that ZnO/CQDs are more effective than ZnO NPs alone for pollutant degradation in aqueous environment.

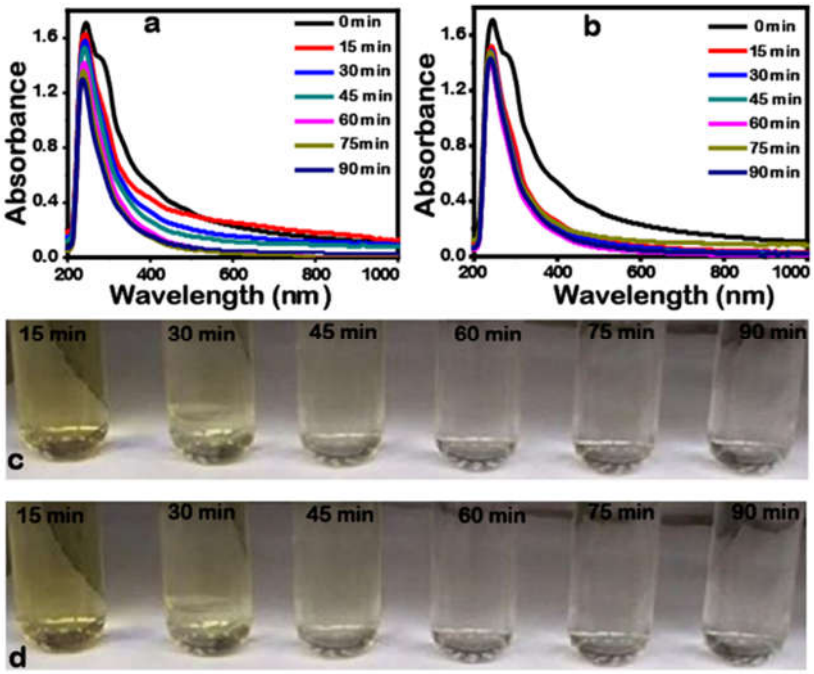

Figure 4. UV-Vis spectra of UHC wastewater at different times of degradation, and their associated pictures using (a, c) ZnO NPs and (b, d) ZnO/CQDs.

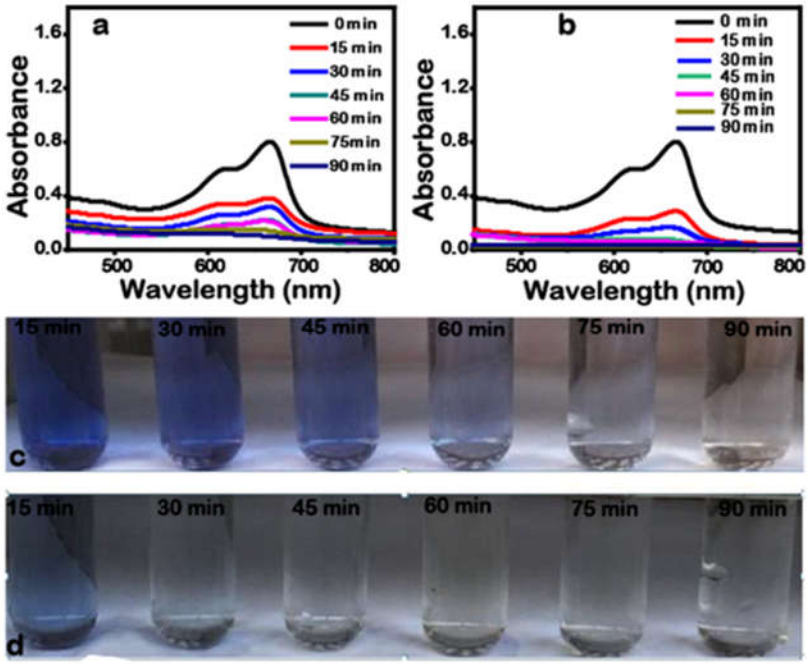

Figure 5. UV-Vis spectra of degradation of 7.5 mg/L MB in UHC wastewater and their associated pictures at different times using (a, c) ZnO NPs and (b, d) ZnO/CQDs.

CONCLUSION

In this work, carbon quantum dots (CQDs) are used to form nanocomposite with zinc oxide nanoparticles (ZnO/CQDs). Evaluation of their photocatalytic properties indicates that the degradation rate of MB follows apparent first-order kinetics. It was found that Langmuir-Hinshelwood type model best describes MB degradation, indicating that the chemical transformation of MB takes place at the surface of the photocatalyst. Furthermore, the study of the photocatalytic properties using ZnO/CQDs displays the best photocatalytic degradation rate which can reach 100% in 45 min while 90 min is needed using ZnO NPs for the complete removal of 7.5 g/L MB under sunlight exposure. This performance seems to be possible due to the reduction of the reflective properties of ZnO NPs in the visible range by the prepared CQDs. This ability of CQDs to improve photocatalytic properties could thus allow ZnO/CQDs to be ideal candidates for the degradation of organic pollutants in general and particularly MB in an aquatic environment under solar irradiation.

REFERENCES

1. Roy, J.S.; Morency, S.; Messaddeq, Y. Ultrafast cleaning of methylene blue contaminated water accelarating photocatalytic reaction rate of the $BiVO_4$ nanoflakes under highly intense sunlight irradiation. *J. Photochem. Photobiol. A* **2021**, 7, 100037-100042.
2. Pimentel, D.; Cooperstein, S.; Randell, H.; Filiberto, D.; Sorrentino, S.; Kaye, B.; Nicklin, C.; Yagi, J.; Brian, J.; O'hern, J. Ecology of increasing diseases: Population growth and environmental degradation. *Hum. Ecol.* **2007**, 35, 653-668.

3. Hasan, H.A.; Abdullah, S.R.S.; Kofli, N.T.; Yeoh, S.J. Interaction of environmental factors on simultaneous biosorption of lead and manganese ions by locally isolated *Bacillus cereus*. *J. Ind. Eng. Chem.* **2016**, 37, 295-305.
4. Laskowski, R.; Bednarska, A.J.; Kramarz, P.E.; Loureiro, S.; Scheil, V.; Kudłek, J.; Holmstrup, M. Interactions between toxic chemicals and natural environmental factors—A meta-analysis and case studies. *Sci. Total Environ.* **2010**, 408, 3763-3774.
5. Matloob, A.; Safdar, M.E.; Abbas, T.; Aslam, F.; Khaliq, A.; Tanveer, A.; Rehman, A.; Chadhar, A.R. Challenges and prospects for weed management in Pakistan: A review. *Crop Protection* **2020**, 134, 104724-104732.
6. Dessalegne, M.; Zewge, F.; Mammo, W.; Woldetinsae, G.; Diaz, I. Effective fluoride adsorption by aluminum oxide modified clays: Ethiopian bentonite vs commercial montmorillonite. *Bull. Chem. Soc. Ethiop.* **2018**, 32, 199-211.
7. Moghaddam, S.S.; Moghaddam, M.A.; Arami, M. Coagulation/flocculation process for dye removal using sludge from water treatment plant: Optimization through response surface methodology. *J. Hazard. Mater.* **2010**, 175, 651-657.
8. Abd Alrazzak, N.; Saad, S.T.; Al-gubury, H.Y.; Kareem, M.M.; Assi, M.M. Photocatalytic degradation efficiency of azo dye in aqueous phase using different photo catalysts. *Bull. Chem. Soc. Ethiop.* **2020**, 34, 463-469.
9. Kim, W.; Tachikawa, T.; Moon, G.h.; Majima, T.; Choi, W. Molecular-level understanding of the photocatalytic activity difference between anatase and rutile nanoparticles. *Angew. Chem. Int. Ed.* **2014**, 126, 14260-14265.
10. Wang, L.-L.; Ren, Z.-Q.; Li, Q. Improvement in optical and electrical properties of ZnO films by neodymium and aluminum co-doping. *J. Mater. Sci. Mater.* **2014**, 25, 2992-2997.
11. Kazeminezhad, I.; Sadollahkhani, A. Photocatalytic degradation of Eriochrome black-T dye using ZnO nanoparticles. *Mater. Lett.* **2014**, 120, 267-270.
12. Dao, D.V.; van den Bremt, M.; Koeller, Z.; Le, T.K. Effect of metal ion doping on the optical properties and the deactivation of photocatalytic activity of ZnO nanopowder for application in sunscreens. *Powder Technol.* **2016**, 288, 366-370.
13. Meshram, S.P.; Adhyapak, P.V.; Pardeshi, S.K.; Mulla, I.S.; Amalnerkar, D.P. Sonochemically generated cerium doped ZnO nanorods for highly efficient photocatalytic dye degradation. *Powder Technol.* **2017**, 318, 120-127.
14. Yibeltal, A.W.; Beyene, B.B.; Admassie, S.; Taddesse, A.M. MWCNTs/Ag-ZnO nanocomposite for efficient photocatalytic degradation of congo red. *Bull. Chem. Soc. Ethiop.* **2020**, 34, 55-66.
15. Kołodziejczak-Radzimska, A.; Jesionowski, T. Zinc oxide—from synthesis to application: A review. *Mater.* **2014**, 7, 2833-2881.
16. Ding, H.; Yu, S.-B.; Wei, J.-S.; Xiong, H.-M. Full-color light-emitting carbon dots with a surface-state-controlled luminescence mechanism. *ACS nano* **2016**, 10, 484-491.
17. Shen, J.; Zhu, Y.; Yang, X.; Li, C. Graphene quantum dots: emergent nanolights for bioimaging, sensors, catalysis and photovoltaic devices. *Chem. commun.* **2012**, 48, 3686-3699.
18. Bozetine, H.; Meziane, S.; Aziri, S.; Berkane, N.; Allam, D.; Boudinar, S.; Hadjersi, T. Facile and green synthesis of a ZnO/CQDs/AgNPs ternary heterostructure photocatalyst: Study of the methylene blue dye photodegradation. *Bull. Mater. Sci.* **2021**, 44, 1-12.
19. Williams, I.B.I.; Kouadio Fodjo, E.; Amadou, K.; Albert, T.; Kong, C. Enhancing the photocatalytic activity of TiO_2 nanoparticles using green carbon quantum dots. *Int. J. Nano Dimens.* **2021**, 13, 144-154.
20. Wang, S.; Zhu, Z.; Chang, Y.; Wang, H.; Yuan, N.; Li, G.; Yu, D.; Jiang, Y. Ammonium hydroxide modulated synthesis of high-quality fluorescent carbon dots for white LEDs with excellent color rendering properties. *Nanotechnology* **2016**, 27, 295202.

21. Ghorbani, H.R.; Mehr, F.P.; Pazoki, H.; Rahmani, B.M. Synthesis of ZnO nanoparticles by precipitation method. *Orient. J. Chem.* **2015**, 31, 1219-1221.
22. Muthulingam, S.; Bae, K.B.; Khan, R.; Lee, I.-H.; Uthirakumar, P. Carbon quantum dots decorated N-doped ZnO: synthesis and enhanced photocatalytic activity on UV, visible and daylight sources with suppressed photocorrosion. *J. Environ. Chem. Eng.* **2016**, 4, 1148-1155.
23. Naushad, M.; Alqadami, A.A.; Al-Kahtani, A.A.; Ahamad, T.; Awual, M.R.; Tatarchuk, T. Adsorption of textile dye using para-aminobenzoic acid modified activated carbon: Kinetic and equilibrium studies. *J. Mol. Liq.* **2019**, 296, 112075-112082.
24. Urbain, K.Y.; Fodjo, E.K.; Ardjouma, D.; Serge, B.Y.; Aimé, E.S.; Marc, G.I.; Albert, T. Removal of imidacloprid using activated carbon produced from ricinodendron heudelotii shells. *Bull. Chem. Soc. Ethiop.* **2017**, 31, 397-409.
25. Kavitha, D.; Namasivayam, C. Experimental and kinetic studies on methylene blue adsorption by coir pith carbon. *Bioresour. Technol.* **2007**, 98, 14-21.
26. Eskalen, H. Influence of carbon quantum dots on electro–optical performance of nematic liquid crystal. *Appl. Phys. A* **2020**, 126, 708-717.
27. Liang, H.; Tai, X.; Du, Z.; Yin, Y. Enhanced photocatalytic activity of ZnO sensitized by carbon quantum dots and application in phenol wastewater. *Opt. Mater.* **2020**, 100, 109674.
28. Gao, D.; Zhao, P.; Lyu, B.; Li, Y.; Hou, Y.; Ma, J. Carbon quantum dots decorated on ZnO nanoparticles: An efficient visible-light responsive antibacterial agents. *Appl. Organomet. Chem.* **2020**, 34, e5665-e5673.
29. Wu, J.; Li, P.; Pan, Y.-T.; Warren, S.; Yin, X.; Yang, H. Surface lattice-engineered bimetallic nanoparticles and their catalytic properties. *Chem. Soc. Rev.* **2012**, 41, 8066-8074.
30. Chen, X.; Wu, Z.; Liu, D.; Gao, Z. Preparation of ZnO photocatalyst for the efficient and rapid photocatalytic degradation of azo dyes. *Nanoscale Res. Lett.* **2017**, 12, 143-152.
31. Jyothi, N.S.; Ravichandran, K. Optimum pH for effective dye degradation: Mo, Mn, Co and Cu doped ZnO photocatalysts in thin film form. *Ceram. Int.* **2020**, 46, 23289-23292.
32. Behnood, R.; Sodeifian, G. Synthesis of N doped-CQDs/Ni doped-ZnO nanocomposites for visible light photodegradation of organic pollutants. *J. Environ. Chem. Eng.* **2020**, 8, 103821-103831.
33. Montazer, M.; Maali Amiri, M. ZnO nano reactor on textiles and polymers: Ex situ and in situ synthesis, application, and characterization. *J. Phys. Chem. B* **2014**, 118, 1453-1470.
34. Moafi, H.F.; Shojaie, A.F.; Zanjanchi, M.A. Semiconductor-assisted self-cleaning polymeric fibers based on zinc oxide nanoparticles. *J. Appl. Polym. Sci.* **2011**, 121, 3641-3650.
35. Ateia, M.; Alalm, M.G.; Awfa, D.; Johnson, M.S.; Yoshimura, C. Modeling the degradation and disinfection of water pollutants by photocatalysts and composites: A critical review. *Sci. Total Environ.* **2020**, 698, 134197-134208.